American Mineralogist, Volume 110, pages 1854–1864, 2025

Crystal chemistry and high-temperature behavior of Al-bearing stishovite and Al-rich phase D: Implications for water storage in the deep mantle

Li Zhang[1,2,*], Joseph R. Smyth[2], and Chaowen Xu[3,4,†]

[1]School of Earth Sciences and Resources, China University of Geosciences, Beijing 100083, China
[2]Department of Geological Sciences, University of Colorado, Boulder, Colorado 80309, U.S.A.
[3]Institute of Earthquake Forecasting, China Earthquake Administration, Beijing 100036, China
[4]Geodynamics Research Center, Ehime University, 2-5 Bunkyo-cho, Matsuyama 7908577, Japan

Abstract

High-quality single crystals of Al-bearing stishovite and Al-rich phase D were analyzed using X-ray diffraction, high-temperature Raman, and FTIR spectroscopy. The samples were synthesized in the MgO-SiO_2-Al_2O_3-H_2O system at 25 GPa, 1350–1600 °C. The results demonstrate that Al-bearing SiO_2 glass formed by the amorphization of stishovite under high-temperature conditions can incorporate water in the form of hydroxyl groups, with a concentration of at least several hundred ppm H_2O by weight. Al^{3+} prefers to enter the crystal structure of phase D by substituting for Si^{4+} in the M2 site. Since Al^{3+} can be charge-balanced by H^+, the Al-rich phase D may have a higher water storage capacity than pure Mg-phase D. Raman and infrared spectral features of Al-rich phase D at ambient temperature can still be observed up to 350 °C. This indicates that, compared to pure Mg-phase D, Al-rich phase D maintains stability at higher temperatures. Al-rich silicate glass formed by the amorphization of phase D under high-temperature conditions can also retain water in the form of hydroxyl groups. In the deep mantle, Al-rich silicate glasses and Al-bearing SiO_2 glasses may serve as potential reservoirs of water (hydrogen) in high-temperature regions beyond the ideal stability fields of dense hydrous magnesium silicates and high-pressure SiO_2 phases.

Keywords: Stishovite, phase D, hydrogen, lower mantle, crystal structure

Introduction

Water (hydrogen) significantly influences the evolution and dynamics of the Earth's interior (e.g., Kohlstedt 2006; Ohtani 2015; Williams and Hemley 2001). Numerous experimental studies have shown that certain constituent minerals in the deep mantle possess a considerable water storage capacity. For instance, wadsleyite and ringwoodite in the mantle transition zone can accommodate a large amount of water (up to 2–3 wt% H_2O) in their crystal structures (e.g., Demouchy et al. 2005; Inoue et al. 1995; Smyth et al. 1997). In addition, natural ringwoodite with 1.4 wt% H_2O was found as an inclusion in a diamond, revealing that the mantle transition zone, at least locally, is wet (Pearson et al. 2014). According to previous investigations on ocean-island basalt (OIB), the source rocks that originated in the lower mantle are commonly water-rich (Dixon et al. 2002; Saal et al. 2002; Pamato et al. 2015). This implies that a suitable host of water also exists in the lower mantle.

Stishovite can be a significant constituent mineral in the subducting oceanic crust, accommodating a substantial amount of water (e.g., Pawley et al. 1993; Chung and Kagi 2002; Bolfan-Casanova et al. 2009; Spektor et al. 2011, 2016; Lin et al. 2020). Various evidence from studies on the mineralogy and composition of the lower mantle supports the existence of this material in the lower mantle (e.g., Stachel et al. 2005; Kaminsky 2012; Litvin et al. 2014; Chen et al. 2020; Deschamps 2024). Although stishovite may contain weight percent levels of H_2O under certain conditions (e.g., Nisr et al. 2017; Lin et al. 2022), recent time-resolved measurements at constant temperatures have shown that the dissolution of water in stishovite is a metastable phenomenon. Therefore, in crustal materials subducting into the lower mantle, stishovite is unlikely to retain >1 wt% of H_2O as a stable phase (Takaichi et al. 2024). FTIR investigations of stishovite samples synthesized at 20–28 GPa and 1200–2100 °C (Litasov et al. 2007; Ishii et al. 2022; Purevjav et al. 2024) indicated that the incorporation of Al^{3+} into stishovite may enhance its water storage capacity. The maximum water contents of Al-bearing samples can be about 3000 wt. ppm H_2O (Litasov et al. 2007). By contrast, the water content of Al-free stishovite samples is below 521 wt. ppm H_2O (Purevjav et al. 2024).

High-pressure and high-temperature experiments have shown that dense hydrous magnesium silicates (DHMS), such as phase A, phase E, superhydrous phase B, phase D, and phase H, can be significant water carriers in subducting slabs (e.g., Frost and Fei 1998; Ohtani et al. 2004; Ohtani 2005; Tsuchiya and Umemoto 2019; Zhang et al. 2019). Among these DHMS, phase D (Liu 1986, 1987; Yang et al. 1997) is stable in the mantle transition zone and at least the shallow parts of the lower mantle (e.g., Shieh et al. 1998; Shinmei et al. 2008; Ghosh and Schmidt 2014; Nishi et al. 2014). At 24 GPa, the maximum thermal stability of phase D is between 1375 and 1400 °C in the MgO-SiO_2-H_2O system, but 1600 °C in the MgO-Al_2O_3-SiO_2-H_2O system. At higher temperatures, phase D is expected to melt, producing a magnesian-rich hydrous melt at the topmost lower mantle (Ghosh and Schmidt, 2014). Pamato et al. (2015) indicated that

* Corresponding author E-mail: li.z.zhang@cugb.edu.cn Orcid https://orcid.org/0000-0001-6337-9001
† Orcid https://orcid.org/0000-0002-8585-5790

0003-004X/25/0011–1854$05.00/DOI: https://doi.org/10.2138/am-2024-9665

hydrous melts formed in the lower mantle can migrate into mafic lithologies and crystallize to form a superaluminous phase D, which is stable at temperatures exceeding 2000 °C at 26 GPa.

In this paper, we analyzed high-quality single crystals of Al-bearing stishovite and Al-rich phase D using X-ray diffraction, high-temperature Raman, and FTIR analyses. The samples were synthesized at 25 GPa and 1350–1600 °C in a MgO-SiO_2-Al_2O_3-H_2O system. Our experimental results provide novel insights into the structural characteristics, water contents, and thermal stabilities of stishovite and phase D in Al-rich regions of the deep mantle, offering new perspectives on water cycling in the Earth's interior.

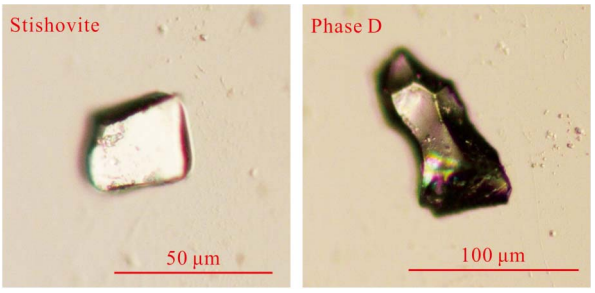

Figure 1. Single-crystal fragments of Al-bearing stishovite ($Si_{0.98}Al_{0.02}O_2$) and Al-rich phase D ($Mg_{0.9}Al_{0.7}Si_{1.3}O_6H_{2.9}$). (Color online.)

Experimental Methods

Sample synthesis

Al-bearing stishovite and coexisting bridgmanite were synthesized at 25 GPa and 1600 °C with a long heating duration of 27 hours in a 1200-ton Sumitomo Kawai-type multi-anvil apparatus at Bayerisches Geoinstitut, University of Bayreuth, Germany. Sintered MgO-Cr_2O_3 pressure media with an octahedral edge length of 7 mm and a $LaCrO_3$ heater in combination with tungsten carbide anvils with 3 mm truncation edge lengths were used (Ishii et al. 2016). Since hydrogen may partition preferentially into melt and hydrous phases during synthesis experiments (e.g., Bolfan-Casanova et al. 2003), the composition of $MgSi_2O_5$ + 2 wt% Al_2O_3 + 1.5 wt% H_2O was prepared as the starting material to minimize the occurrence of melt and hydrous phases (such as phase D and phase Egg). Starting materials were mixed from high-purity MgO, SiO_2, Al_2O_3, and $Mg(OH)_2$ and were sealed into a Pt capsule before being placed into the experimental assembly. After sample synthesis, the recovered capsule was mounted in epoxy on a round glass slide and ground to expose the run product (Online Materials[1] Fig. S1). Single crystals of Al-rich phase D were previously synthesized by a Kawai-type (MA-8-type) high-pressure apparatus at Geodynamics Research Center, Ehime University (Xu and Inoue 2019). The compositions of about $MgAl_{0.7}Si_{1.3}O_6H_{2.7}$ were prepared as starting materials. The samples used in this study were synthesized at 25 GPa, 1350 °C and 25 GPa, 1000 °C. More details of the sample syntheses were reported by Xu and Inoue (2019).

Electron microprobe analysis

The chemical compositions of the coexisting stishovite and bridgmanite (Online Materials[1] Fig. S1) were examined using a JEOL 8900 electron microprobe with a 15 kV accelerating voltage, 5 nA beam current, 5 μm probe diameter, using natural or synthetic standards. The chemical compositions of the phase D samples were reported in Xu and Inoue (2019). Assuming a total sum of 100 wt%, their formula units are estimated to be $Mg_{0.9}Al_{0.7}Si_{1.3}O_6$ $H_{2.9}$ (phase D synthesized at 25 GPa and 1350 °C) and $Mg_{0.93}Al_{0.7}Si_{1.28}O_6H_{2.91}$ (phase D synthesized at 25 GPa and 1000 °C), respectively.

Single-crystal X-ray diffraction

Single crystals (Fig. 1) of Al-bearing stishovite and Al-rich phase D were respectively mounted on glass fibers and centered for X-ray diffraction analysis. Intensity data were collected with a Bruker D8 Venture diffractometer equipped with a Photon II detector. X-ray (calibrated radiation λ = 0.71073 Å) was generated by a IμS 3.0 generator using a rotating Mo-anode. Crystal structures were refined from the intensity data sets using SHELXL-2018 (Sheldrick 2018) in the package WINGX (Farrugia 1999). Scattering factors and absorption coefficients for Mg, Si, Al, and O from *International Tables for Crystallography, Volume C* (Prince 2004) were used. The crystal structure refinement results are provided in a CIF[1] within the Online Materials[1].

High-temperature raman spectroscopy

The ambient laser Raman spectra of the selected single crystals were collected by a WITec's confocal Raman imaging microscope (alpha300R). The spectra were excited at 40 mW power and by a 532 nm diode-pumped solid-state laser with a spectral resolution of 1 cm^{-1}, using 1800 gr/mm grating. The focused laser spot was 1 μm in diameter on the sample. All bands were recorded from randomly oriented specimens with a 50× microscope objective, using five accumulations with 10 s exposure time. For high-temperature measurements, the spectra were recorded in the temperature range of 25–600 °C at 50 °C intervals by using a Linkam TS1400 heating stage with a SiO_2 window and a Rh/Pt thermocouple. The single-crystal samples were placed on a sapphire substrate. At each temperature, the samples were held for at least 15 min to attain thermal equilibrium. During data collection, the increasing and decreasing rates of temperature were 30 °C/min and −30 °C/min, respectively.

High-temperature FTIR spectroscopy

Doubly polished single-crystal samples were prepared for Fourier Transform Infrared Spectrometer (FTIR) analyses. Unpolarized infrared spectra were obtained using a Bruker INVENIO-R FTIR spectrometer with a 20× objective on the HYPERION 1000 microscope, CaF_2 beam-splitter, and a MCT detector. For each spectrum, 128 or 256 scans were accumulated with a resolution of 2 cm^{-1} and 30×30 μm aperture. The measurements at ambient conditions were done by placing the crystals on a KBr plate. Water contents of nominally anhydrous minerals were estimated based on the Beer-Lambert law (e.g., Koch-Müller and Rhede 2010; Thomas et al. 2015; Zhu et al. 2023):

$$C_{H_2O} = (A_i \times 1.8)/(t \times d \times \varepsilon_i) \quad (1)$$

where C_{H_2O} is the water content in wt% H_2O, A_i is the absorbance area of the OH band in cm^{-1}, t is the sample thickness in centimeters, d is the sample density in g/cm^3, ε_i is the integral molar absorption coefficient in $L/mol(H_2O)/cm^{-2}$. The total absorbance should be the sum of the absorbance in all three polarization directions of a crystal (Libowitzky and Rossman 1997). For non-polarized infrared spectroscopy measurements, the total absorbance can be estimated by multiplying the absorbance of the OH bands in the infrared spectrum by a factor of three (e.g., Libowitzky and Rossman 1996; Purevjav et al. 2024). For high-temperature measurements, a Linkam TS1400 heating stage with a ZnSe window and a Rh/Pt thermocouple was employed. The spectra were recorded over a temperature range of 25 to 600 °C at 50 °C intervals. The increasing and decreasing rates of temperature were 30 and −30 °C/min, respectively. During data collection, the samples were placed on a sapphire substrate and held at each temperature for at least 15 min to reach equilibrium.

Results and Discussion

Stishovite

Our results of chemical composition analysis show that stishovite and bridgmanite contain 1.9 and 2.5 wt% Al_2O_3, respectively (Table 1). Previous studies (e.g., Smyth et al. 1995; Litasov et al. 2007) have shown that the unit-cell volume of stishovite increases with increasing Al_2O_3 content. The structure refinement indicates that the unit-cell volume (46.86 $Å^3$) of the Al-bearing stishovite in this study (Table 2) is slightly larger than that (46.46–46.51 $Å^3$) of pure SiO_2 stishovite (Smyth et al. 1995; Litasov et al. 2007). This result is in good agreement with the previously reported data for stishovites (Smyth et al. 1995; Litasov et al. 2007).

Table 1. Experimental conditions and chemical compositions of the samples

Sample[a]	*P* (GPa)	*T* (°C)	Time (h)	MgO (wt%)	SiO_2 (wt%)	Al_2O_3 (wt%)	Total (wt%)
Stishovite	25	1600	27	–	98.39(87)	1.89(3)	100.28(84)
Bridgmanite				38.56(28)	59.06(48)	2.46(3)	100.07(68)
Phase D (sample 1)	25	1350	1	21.31(25)	43.59(42)	20.24(24)	85.14(32)
Phase D (sample 2)	25	1000	7	21.45(88)	43.94(51)	20.35(10)	85.73(177)

[a] The chemical compositions of the phase D samples were referred to Xu and Inoue (2019).

Table 2. Structural refinement details, unit-cell parameters, atomic coordinates, and site geometry parameters for Al-bearing stishovite

Structural refinement details			
Measured reflections	745	Max. 2θ	60.1°
Unique reflections	48	R_{all}	0.0447
*wR*2	0.0825	R_w for $F_o > 4\sigma(F_o)$	0.0379
R_{int}	0.0398	*GooF*	1.254
Unit-cell parameters and space group			
a	*c*	Volume	Space group
4.1885(9) Å	2.6712(6) Å	46.86(2) Å^3	$P4_2/mnm$
Atomic coordinates			
	X	*Y*	*Z*
Si	0	0	0
O	0.3060(7)	0.3060(7)	0
Site geometry parameters			
Si-O(4)	1.762(2) Å	Volume	7.4185 Å^3
Si-O(2)	1.813(3) Å	OAV	26.7871
Mean Si-O	1.7788 Å	QE	1.0079

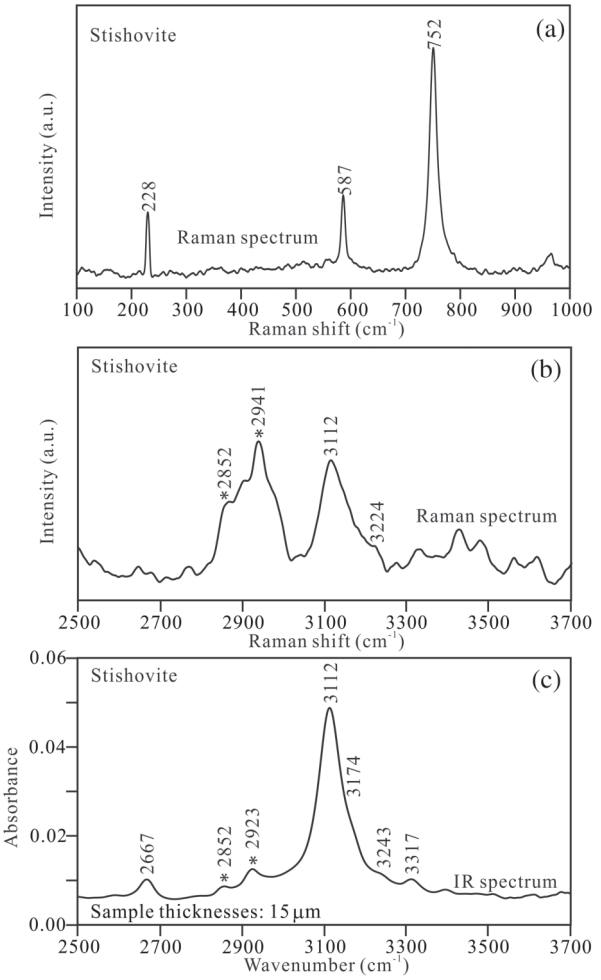

Figure 2. Representative Raman and infrared spectra of Al-bearing stishovite at ambient conditions: (**a**) Raman spectrum in the wavenumber range of 100–1000 cm^{-1}; (**b**) Raman spectrum in the OH vibration region; (**c**) infrared spectrum in the OH vibration region. The asterisks represent the bands that are assigned to minor residual acetone or adhesive.

At ambient temperature, the Raman spectrum of the Al-bearing stishovite in this study has major bands at 228, 587, and 752 cm^{-1} in the wavenumber range of 100–1000 cm^{-1} (Fig. 2). This is consistent with previous data (e.g., Liu et al. 1997; Spektor et al. 2016). The infrared spectrum at ambient conditions displays one major band at 3112 cm^{-1} and some additional bands at 2667, 3174, 3243, and 3317 cm^{-1} in the OH vibration region (Fig. 2c), implying multiple mechanisms for H incorporation. The bands at 2852 and 2923 cm^{-1} (at 2852 and 2941 cm^{-1} in the Raman spectrum) indicate minor residual acetone or adhesive, which cannot be removed by drying the sample (Litasov et al. 2007; Panero et al. 2013). The two bands at 3112 and 3174 cm^{-1} are very close to each other and have identical anisotropies (Bromiley et al. 2006; Litasov et al. 2007). They are both assigned to the H at a position near the shortest O-O edge (2.298 Å) of the octahedra (Smyth et al. 1995; Bromiley et al. 2006; Litasov et al. 2007). The strong 3112 cm^{-1} band can be observed in the spectra of both Al-free and Al-bearing stishovites (Bromiley et al. 2006; Litasov et al. 2007; Purevjav et al. 2024). It is therefore expected to be associated with H^+, not coupled to Al^{3+} substitutional defect on the adjacent octahedral site. By contrast, the 3174 cm^{-1} band is only present in the spectra of Al-bearing stishovite. Thus, it can be due to the coupled substitution of H^+ and Al^{3+} on the octahedral site (Bromiley et al. 2006). The 3317 cm^{-1} band is also associated with Al^{3+} substitutional defects, whereas it corresponds to the vibration of hydroxyls toward interstitial sites in the crystal structure (Litasov et al. 2007). The band at 3243 cm^{-1} was rarely observed in the previously reported spectra of Al-rich stishovite. This may be related to interstitial H^+ associated with Si^{4+} vacancies (Bromiley et al. 2006; Litasov et al. 2007). The relatively low wavenumber of the 2667 cm^{-1} band implies a strong hydrogen bond interaction (Libowitzky 1999). Spektor et al. (2011) suggested that this band is related to the hydrogarnet-like defect where four H^+ replace one Si^{4+} in the octahedral site. The four O atoms around this silicon vacancy are terminated as hydroxyl. The two remaining underbonded O atoms act as acceptors for strong H bonds (Spektor et al. 2011, 2016).

In the Raman spectra of the Al-bearing stishovite samples (Fig. 2b), the intense OH band at 3112 cm^{-1} is also observed. The peaks (at 2850–2940 cm^{-1}) caused by residual acetone or adhesive (Litasov et al. 2007; Panero et al. 2013) show markedly higher intensities in the Raman spectra compared to

those in the infrared spectra (Fig. 2). This may result from the reduced interference of surface-localized contaminants on infrared transmitted light. As shown in Figure 2b, a series of weak peaks can be observed in the 3400–3700 cm^{-1} region of the Raman spectra. However, these peaks were not detected in either the infrared spectra collected in this study (Fig. 2c) or those reported in previous research (Bromiley et al. 2006; Litasov et al. 2007; Purevjav et al. 2024). Furthermore, the relative intensities, positions, and resolutions of the Raman spectra obtained from different sample fragments exhibit significant variations. Therefore, they may be attributed to background interference peaks.

The water content of the Al-bearing stishovite in this study is estimated to be ~320 wt. ppm H_2O, based on the integrated molar absorption coefficient [163 000 ± 120 000 L/mol(H_2O)/cm^{-2}] reported in prior literature (Pawley et al. 1993; Litasov et al. 2007). The value is very similar to that (about 370 wt. ppm H_2O) of the reported Al-bearing single-crystal sample (contains 2.1 wt% Al_2O_3) synthesized with bridgmanite at 25 GPa and 1200 °C under hydrous conditions (Litasov et al. 2007). Unpolarized Raman and infrared spectra at ambient conditions (Online Materials[1] Fig. S2) imply that the Al-bearing bridgmanite, which coexists with Al-bearing stishovite in this study, is nearly dry.

The Raman spectra of the Al-bearing stishovite in this study as a function of increasing and decreasing temperature in the range of 25–600 °C are shown in Figure 3. The four Raman bands shift continuously to lower frequencies as the temperature increases. At the temperature of 600 °C, a significant decrease in the intensity of the major Raman bands at 228 (ν_4) and 752 cm^{-1} (ν_2) can be observed. By contrast, a broad band at about 495 cm^{-1} becomes the most intense band in the Raman spectra (Fig. 3), implying the amorphization of the Al-bearing stishovite. This

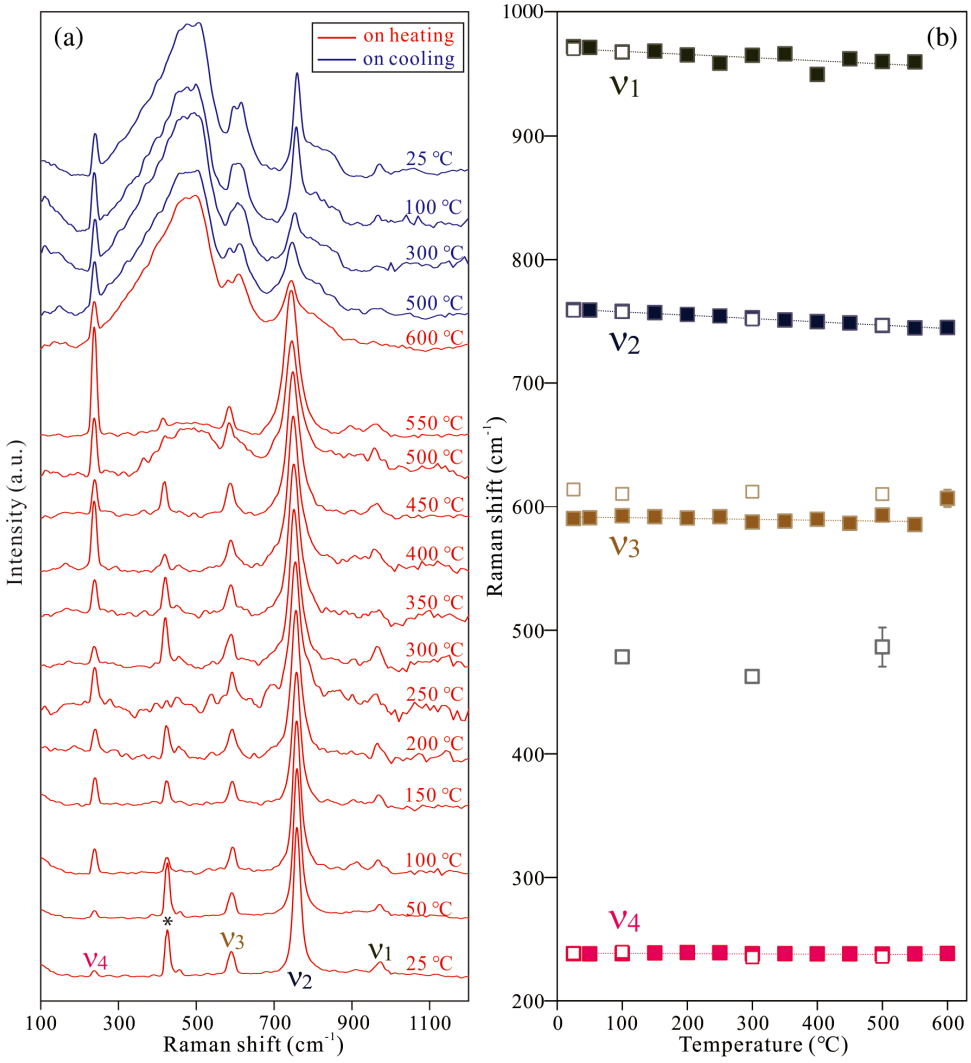

Figure 3. (**a**) Raman spectra of Al-bearing stishovite as a function of increasing and decreasing temperature at 1 atm. (**b**) Frequency shifts of the Raman bands during heating (filled squares) and cooling (open squares). Error bars are provided for bands with errors exceeding the symbol size. Temperature derivatives of ν_1, ν_2, ν_3, and ν_4 are estimated to be −0.025(6), −0.027(1), −0.007(4), and −0.002(1) cm^{-1}/°C, respectively, based on data collected during heating. The asterisk represents the band that is assigned to the sapphire substrate (Litasov et al. 2007; Panero et al. 2013). (Color online.)

result is consistent with the high-temperature Raman scattering investigations of pure SiO_2 stishovite (e.g., Grimsditch et al. 1994; Liu et al. 1997). However, previous studies did not report the spectral features of stishovite in the OH vibration region at elevated temperatures.

The high-temperature FTIR analysis of the Al-bearing stishovite in this study (Fig. 4) shows that the OH bands at 2667 (ν_6), 3016 (ν_4), and 3112 cm^{-1} (ν_3) shift to lower frequencies with increasing temperature. By contrast, the two weak bands at 3243 (ν_2) and 3317 cm^{-1} (ν_1) shift to higher wavenumbers in the OH stretching region upon heating (Fig. 4), implying the weakening of the hydrogen bond interactions. This phenomenon can be explained by the increasing O-O distances between adjacent octahedra with increasing temperature. During heating, the broadening of the major 3112 cm^{-1} (ν_3) band within the investigated temperature range can be observed. As a result, the frequencies of the 3174 cm^{-1} band cannot be recorded (Fig. 4). Due to the temperature-induced amorphization of the Al-bearing stishovite at 600 °C, the band at 2667 cm^{-1} (ν_6) shifts abruptly to a frequency of about 2505 cm^{-1}. In addition, a new intense band appears at approximately 2970 cm^{-1}. However, the frequency changes of the bands are reversible during cooling. Although the background feature of the infrared spectrum differs from that of the initial spectrum before heating, the strong IR bands at about 3112 (ν_3) and 2665 cm^{-1} (ν_6) can be observed at ambient temperature after cooling (Fig. 4). This indicates that high-temperature SiO_2 glass, formed by the amorphization of Al-bearing stishovite under high-temperature conditions, can incorporate water in the form of hydroxyl groups, with a concentration of at least several hundred ppm wt. H_2O.

Phase D

The single-crystal X-ray diffraction data for the Al-rich Phase D samples are presented in Table 3 and Online Materials[1] Table S1. The crystal structure of phase D is based on a hexagonal closest-packed array of O atoms. All cations except H are located in octahedrally coordinated sites, which occur in two separate layers stacked along the *c*-axis (Yang et al. 1997; Boffa Ballaran et al. 2010). In Al-free phase D (Mg-phase D), the sites corresponding to the 1*a* (M1 site) and 2*d* (M2 site) Wyckoff

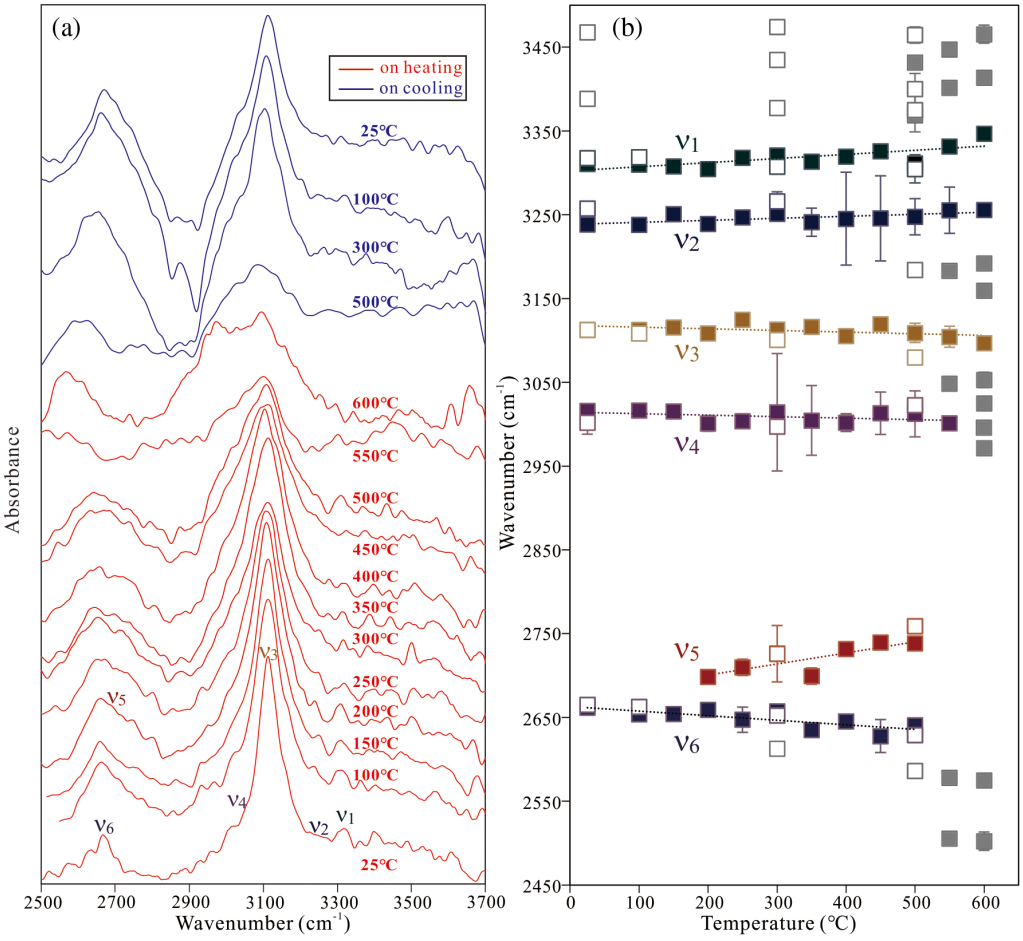

Figure 4. (**a**) Unpolarized infrared spectra of Al-bearing stishovite as a function of increasing and decreasing temperature at 1 atm. (**b**) Frequency shifts of the IR bands during heating (filled squares) and cooling (open squares). Error bars are provided for bands with errors exceeding the symbol size. Temperature derivatives of ν_1, ν_2, ν_3, ν_4, ν_5, and ν_6 are estimated to be 0.050(13), 0.024(8), −0.02(1), −0.017(11), 0.132(43), and −0.054(16) cm^{-1}/°C, respectively, based on data collected during heating. (Color online.)

Table 3. Structural refinement details, unit-cell parameters, and atomic coordinates for Al-rich phase D

		Structural refinement details		
Sample 1	Measured reflections	2550	Max. 2θ	59.01°
	Unique reflections	97	R_{all}	0.0366
	*wR*2	0.1269	R_w for $F_o > 4\sigma(F_o)$	0.0364
	R_{int}	0.0218	*GooF*	1.385
Sample 2	Measured reflections	2717	Max. 2θ	58.98°
	Unique reflections	99	R_{all}	0.0315
	*wR*2	0.1095	R_w for $F_o > 4\sigma(F_o)$	0.0301
	R_{int}	0.0202	*GooF*	1.428
		Unit-cell parameters and space group		
Sample 1	*a*	*c*	Volume	Space group
	4.8222(4) Å	4.2989(6) Å	86.572(19) Å	$P\bar{3}1m$
Sample 2	*a*	*c*	Volume	Space group
	4.8226(4) Å	4.3042(5)	86.693(18)	$P\bar{3}1m$
		Atomic coordinates		
		X	*Y*	*Z*
Sample 1	M1(Mg)	0	0	0
	M2(Si)	1/3	2/3	1/2
	O	0.6348(4)	0	0.2639(4)
Sample 2	M1(Mg)	0	0	0
	M2(Si)	1/3	2/3	1/2
	O	0.6336(5)	0	0.2645(5)

Notes: Sample 1 and sample 2 were synthesized at 25 GPa, 1350 °C and 25 GPa, 1000 °C (Xu and Inoue 2019), respectively. Site geometry parameters for Al-rich phase D are provided in Online Materials[1] Table S1.

Table 4. Selected interatomic distances of phase D

Sample	Formula unit[a]	M1–O distance (Å)	M2–O distance (Å)	M3–O distance (Å)
Al-free phase D (Yang et al. 1997)	$Mg_{1.11}Si_{1.89}O_6H_{2.22}$	2.1050(9)	1.8050(6)	–
Al-rich phase D (This study)	$Mg_{0.93}Al_{0.7}Si_{1.28}O_6H_{2.91}$	2.1020(20)	1.8386(14)	–
Al-rich phase D (This study)	$Mg_{0.9}Al_{0.7}Si_{1.3}O_6H_{2.9}$	2.0948(19)	1.8414(11)	–
Al-dominant phase D (Boffa Ballaran et al. 2010)	$Mg_{0.2}Fe_{0.12}Al_{1.5}Si_{0.92}O_6H_{3.1}$	1.9197(17)	1.9151(12)	1.9150(10)

[a] The results of previously reported EMPA analyses.

positions are occupied by Mg and Si, respectively. The sites corresponding to the 2*c* (M3 site) and 1*b* positions are vacant (Yang et al. 1997; Boffa Ballaran et al. 2010). By comparison, in Al-dominant phase D (contains 43.1 wt% Al_2O_3), Si and Al can enter into the M1, M2, and M3 site. Although it is difficult to determine the site occupancies of the atoms that have similar scattering factors, the same cation-oxygen distances of all sites (Table 4) indicate a high degree of Si/Al disorder in Al-dominant phase D (Boffa Ballaran et al. 2010). The structure refinement (Table 3; Online Materials[1] Table S1) in this study shows that the M3 site is vacant in the crystal structure of Al-rich phase D samples (containing 20.24–20.35 wt% Al_2O_3). As presented in Table 4 and Online Materials[1] Table S1, the M1-O distances of Al-rich and Mg-phase D are very similar. By contrast, the

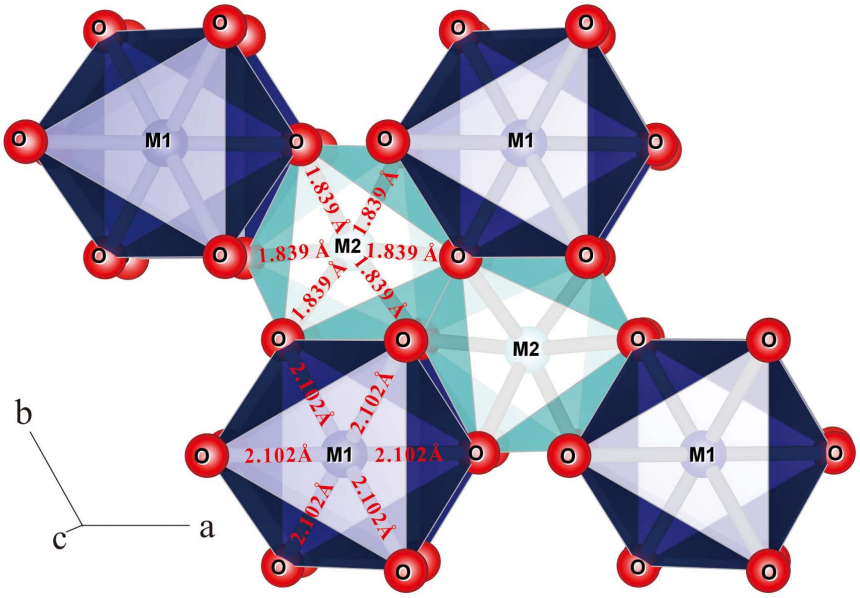

Figure 5. Structural model of Al-rich phase D. The M1 octahedral site is occupied by Mg and Al. The M2 octahedral site is occupied by Si and Al. The M1-O and M2-O bond distances are indicated. (Color online.)

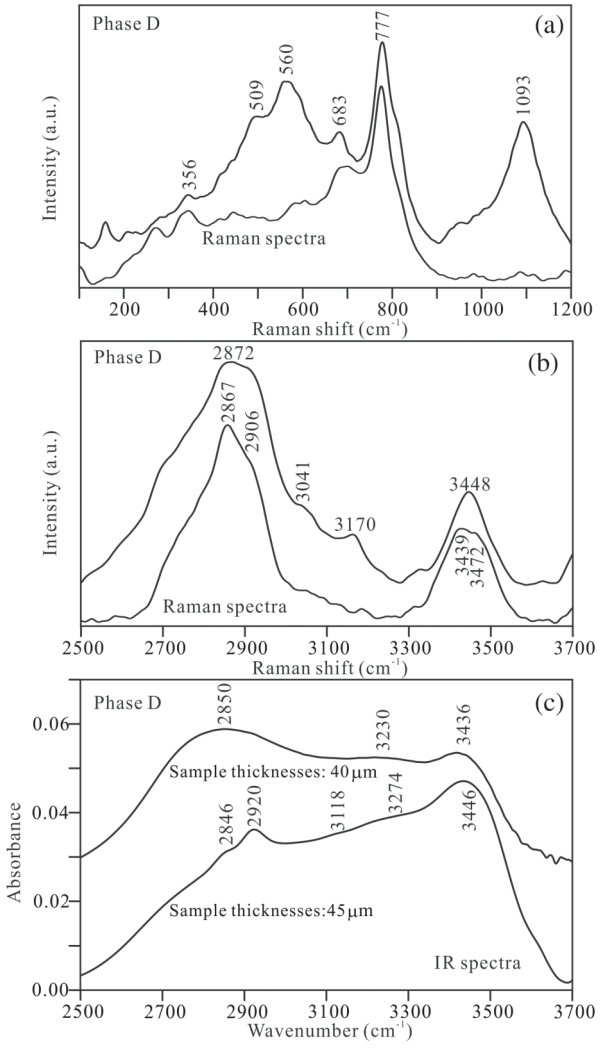

Figure 6. Representative Raman and infrared spectra of Al-rich phase D at ambient conditions. (**a**) Raman spectra in the wavenumber range of 100–1200 cm^{-1}. (**b**) Raman spectra in the OH vibration region. (**c**) infrared spectra in the OH vibration region.

M2-O distance [1.8386(14)−1.8414(11) Å] of Al-rich phase D is significantly longer than that [1.8050(6) Å] of Mg-phase D (Table 4), indicating that Al^{3+} prefers entering into the crystal structure of phase D by substitution for Si^{4+} in the M2 site (Fig. 5). This result is consistent with the EMPA analyses. To satisfy the electro-neutrality requirement, Al^{3+} can be charge-balanced by H^{+}. Therefore, Al-rich phase D is expected to have a higher water storage capacity than pure Mg-phase D.

The representative Raman and infrared spectra of the Al-rich phase D samples (the spectral features of the two samples are consistent, as listed in Table 1) under ambient conditions are shown in Figure 6. The frequencies of the Raman bands observed in the range of 100−1200 cm^{-1} are in general agreement with the data for phase D reported previously (Liu et al. 1998; Boffa Ballaran et al. 2010; Xu and Inoue 2019). The intensities of the Raman bands at about 560 and 1093 cm^{-1} vary from sample to sample (Fig. 6), implying that these bands are highly anisotropic. The Raman and infrared spectra in the 2800−3450 cm^{-1} region display a group of broad O-H stretching bands, indicating the disorder of the hydrogen positions. This spectral feature is consistent with previous observations (Yang et al. 1997; Shieh et al. 2009; Boffa Ballaran et al. 2010).

Figures 7 and 8 show the Raman and infrared spectra of the Al-rich phase D samples as a function of temperature in the range of 25−600 °C. The four Raman bands (Fig. 7) and the IR band at about 3500 cm^{-1} (ν_1) (Fig. 8) exhibit a linear shift with increasing temperature up to 350 °C. In contrast, the three IR bands at about 2850 (ν_4), 2925 (ν_3), and 3400 cm^{-1} (ν_2) shift nonlinearly toward higher frequencies (Fig. 8). The observed nonlinear behavior of these bands may be related to the band broadening or the slight frequency shifts within the investigated temperature range. For the IR bands in the 3000−3300 cm^{-1} region, the trends of frequency variations cannot be recorded at higher temperatures, since the resolutions of these broad bands are very poor (Fig. 8). Liu et al. (1998) suggested that amorphization of pure Mg-phase D may take place above 100 °C at atmospheric pressure. However, all the Raman and infrared spectral features of the Al-rich phase D sample in this study at ambient temperature can still be observed up to 350 °C (Figs. 7 and 8), implying that Al-rich phase D maintains stability at higher temperatures compared to pure Mg-phase D.

At temperatures above 400 °C, a significant decrease in the intensity of the major Raman band at 777 cm^{-1} (ν_1) can be observed. By contrast, the band at about 165 cm^{-1} emerges in the Raman spectra and becomes the most intense band at about 600 °C (Fig. 7), indicating the temperature-induced amorphization of the crystal structure. As shown in Fig. 8, a group of stronger and broader bands at about 3300–3650 cm^{-1} emerges in the infrared spectra due to the amorphization. All these bands can be observed evidently to the highest temperature (600 °C) and exhibit a negative shift to 25 °C without notable change in intensity during cooling (Fig. 8). They cannot be due to molecular H_2O released by dehydration, since the infrared spectrum of liquid water at ambient conditions is characterized by a single broad band at about 3400 cm^{-1} (Johnson and Rossman 2003, 2004). As shown in Figure 8, the most intense bands in the infrared spectrum of our sample are seen at about 3550−3610 cm^{-1} at ambient temperature after cooling. Although these bands were not observable in the previously reported infrared spectra of phase D, they are assigned to structural OH in some other minerals and indicate a wider range of hydrogen bonding distances resulting from structural damage (Johnson 2006). Therefore, we attribute the broader bands at temperatures above 400 °C to the presence of hydroxyl groups. The results of our spectroscopic analysis indicate that high-temperature silicate glass, formed by the amorphization of Al-rich phase D, can also retain water in the form of hydroxyl groups.

Implications

High-temperature Raman spectroscopy analysis indicates that Al-bearing stishovite can undergo amorphization at 550 °C,

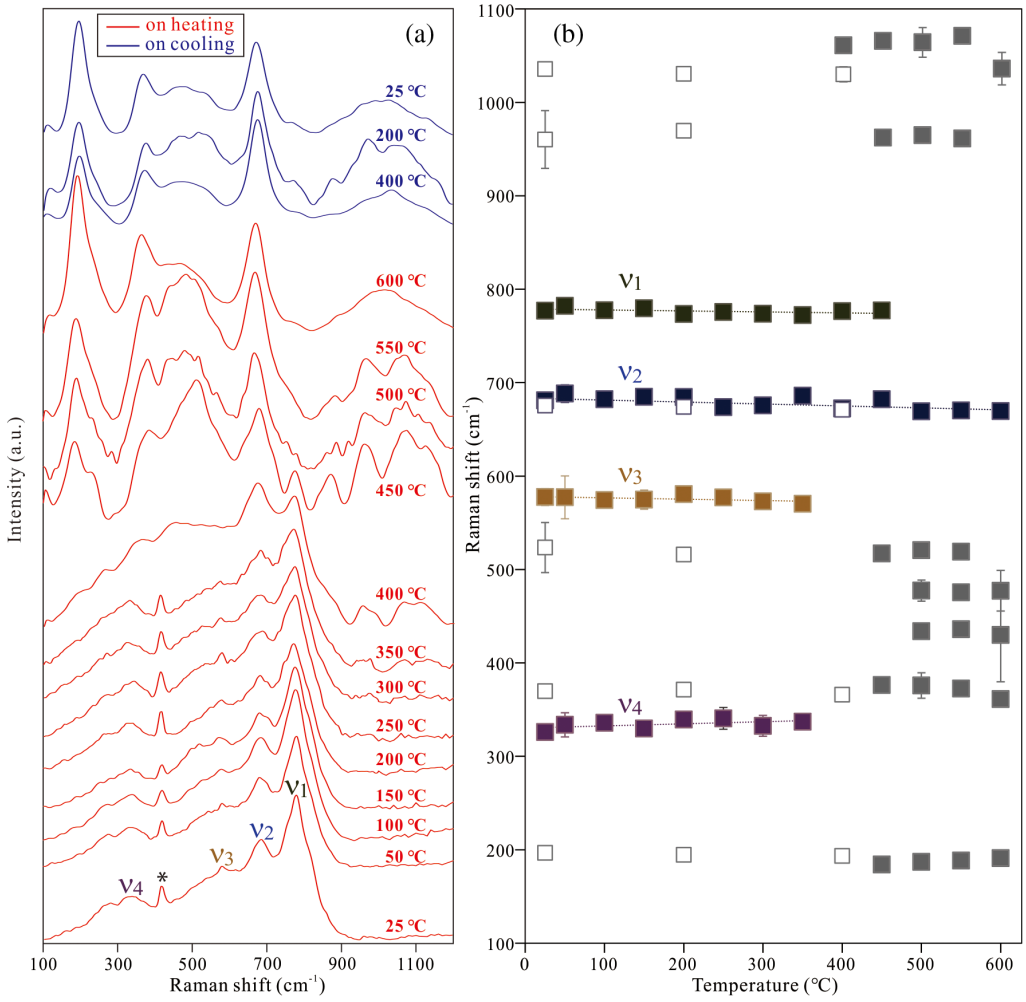

FIGURE 7. (**a**) Raman spectra of Al-rich phase D as a function of increasing and decreasing temperature at 1 atm. (**b**) Frequency shifts of the Raman bands during heating (filled squares) and cooling (open squares). Error bars are provided for bands with errors exceeding the symbol size. Temperature derivatives of ν_1, ν_2, ν_3, and ν_4 are estimated to be −0.010(6), −0.021(7), −0.014(9), and 0.022(14) cm^{-1}/°C, respectively, based on data collected during heating. The asterisk represents the band that is assigned to the sapphire substrate. (Color online.)

transforming into SiO_2 glass. However, the frequency changes of the infrared bands in the OH vibration region are reversible during cooling. The strong OH bands at about 3112 and 2665 cm^{-1} can be observed at 25 °C after cooling. This reveals that the high-temperature SiO_2 glass still retains several hundred ppm wt. H_2O. Single-crystal X-ray diffraction analysis of Al-rich phase D indicates that Al^{3+} prefers entering into the crystal structure by substitution for Si^{4+} in the M2 site. To satisfy the electro-neutrality requirement, Al^{3+} is expected to be charge-balanced by H^+. Thus, Al-rich phase D may have a higher water storage capacity than Al-free phase D (Mg-phase D). High-temperature Raman and FTIR analyses demonstrate that Al-rich phase D exhibits stability at higher temperatures compared to pure Mg-phase D. Additionally, Al-rich silicate glass formed by the amorphization of phase D can also retain water in the form of hydroxyl groups. This implies that temperature-induced amorphization may not directly trigger the dehydration of Al-rich phase D in the deep mantle.

Our experimental results suggest that Al-rich silicate glasses and Al-bearing SiO_2 glasses may serve as potential reservoirs of water (hydrogen) in the lower mantle. These glasses can form respectively by the amorphization of Al-rich DHMS and Al-bearing SiO_2 phases, retaining significant amounts of hydrogen in the form of hydroxyl groups within high-temperature regions beyond the ideal stability fields of their precursor DHMS and SiO_2 phases. Consequently, they may also participate in deep-water cycling processes within the Earth's interior, thereby influencing the structure and physical properties of the lower mantle. Recent research (Tsutsumi et al. 2024) revealed that, due to the high water-storage capacity of the SiO_2 phase and SiO_2-AlOOH solid solution under the high-temperature conditions of the core-mantle boundary, water does not escape from subducted slabs. Consequently, the formation of low-velocity anomalies observed in the large low shear velocity provinces (LLSVPs) cannot be attributed to hydration around these slabs. Our research findings imply that the presence of Al-rich silicate

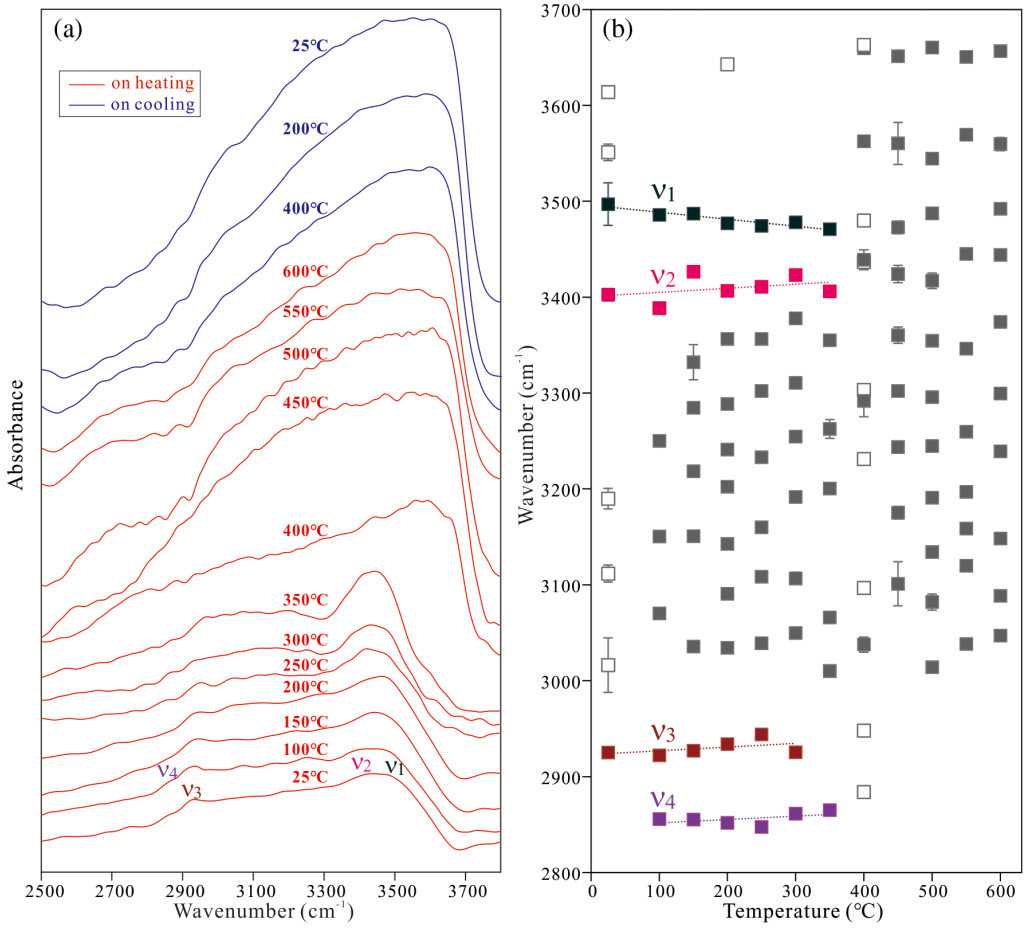

Figure 8. (**a**) Unpolarized infrared spectra of Al-rich phase D as a function of increasing and decreasing temperature at 1 atm. (**b**) Frequency shifts of the IR bands during heating (filled squares) and cooling (open squares). Error bars are provided for bands with errors exceeding the symbol size. Temperature derivatives of ν_1, ν_2, ν_3, and ν_4 are estimated to be −0.073(13), 0.043(46), 0.038(35), and 0.035(29) $cm^{-1}/°C$, respectively, based on data collected during heating. (Color online.)

glasses and Al-bearing SiO_2 glasses may also contribute to the retention of water in subducted slabs.

Data Availability

All the data are available and can be found in Figures 1–8, Tables 1–4, and the Online Materials[1].

Acknowledgements and Funding

This study was supported by the National Natural Science Foundation of China (No. 42172044 to L.Z. and No. 42003050 to C.X.), and U.S. National Science Foundation (Grant EAR 14-16979 to J.R.S.)

References Cited

Boffa Ballaran, T., Frost, D.J., Miyajima, N., and Heidelbach, F. (2010) The structure of a super-aluminous version of the dense hydrous-magnesium silicate phase D. American Mineralogist, 95, 1113–1116, https://doi.org/10.2138/am.2010.3462.

Bolfan-Casanova, N., Keppler, H., and Rubie, D.C. (2003) Water partitioning at 660 km depth and evidence for very low water solubility in magnesium silicate perovskite. Geophysical Research Letters, 30, 1905, https://doi.org/10.1029/2003GL017182.

Bolfan-Casanova, N., Andrault, D., Amiguet, E., and Guignot, N. (2009) Equation of state and post-stishovite transformation of Al-bearing silica up to 100 GPa and 3000 K. Physics of the Earth and Planetary Interiors, 174, 70–77, https://doi.org/10.1016/j.pepi.2008.06.024.

Bromiley, G.D., Bromiley, F.A., and Bromiley, D.W. (2006) On the mechanisms for H and Al incorporation in stishovite. Physics and Chemistry of Minerals, 33, 613–621, https://doi.org/10.1007/s00269-006-0107-9.

Chen, H.W., Leinenweber, K., Prakapenka, V., Kunz, M., Bechtel, H.A., Liu, Z., and Shim, S.-H. (2020) Phase transformation of hydrous ringwoodite to the lower-mantle phases and the formation of dense hydrous silica. American Mineralogist, 105, 1342–1348, https://doi.org/10.2138/am-2020-7261.

Chung, J.I., and Kagi, H. (2002). High concentration of water in stishovite in the MORB system. Geophysical Research Letters, 29, 16-1–16-4, https://doi.org/10.1029/2002GL015579.

Demouchy, S., Deloule, E., Frost, D.J., and Keppler, H. (2005) Pressure and temperature dependence of water solubility in iron-free wadsleyite. American Mineralogist, 90, 1084–1091, https://doi.org/10.2138/am.2005.1751.

Deschamps, F. (2024) Deep mantle water prefers slabs. Nature Geoscience, 17, 590–591, https://doi.org/10.1038/s41561-024-01468-4.

Dixon, J.E., Leist, L., Langmuir, C., and Schilling, J.G. (2002) Recycled dehydrated lithosphere observed in plume-influenced mid-ocean-ridge basalt. Nature, 420, 385–389, https://doi.org/10.1038/nature01215.

Farrugia, L.J. (1999) WinGX suite for small-molecule single-crystal crystallography. Journal of Applied Crystallography, 32, 837–838, https://doi.org/10.1107/S0021889899006020.

Frost, D.J. and Fei, Y. (1998) Stability of phase D at high pressure and high temperature. Journal of Geophysical Research: Solid Earth, 103, 7463–7474, https://doi.org/10.1029/98JB00077.

Ghosh, S. and Schmidt, M.W. (2014) Melting of phase D in the lower mantle and implications for recycling and storage of H_2O in the deep mantle. Geochimica et Cosmochimica Acta, 145, 72–88, https://doi.org/10.1016/j.gca.2014.06.025.

Grimsditch, M., Popova, S., Brazhkin, V.V., and Voloshin, R.N. (1994) Temperature-induced amorphization of SiO_2 stishovite. Physical Review B: Condensed Matter, 50, 12984–12986, https://doi.org/10.1103/PhysRevB.50.12984.

Inoue, T., Yurimoto, H., and Kudoh, Y. (1995) Hydrous modified spinel, $Mg_{1.75}SiH_{0.5}O_4$: A new water reservoir in the mantle transition region. Geophysical Research Letters, 22, 117–120, https://doi.org/10.1029/94GL02965.

Ishii, T., Shi, L., Huang, R., Tsujino, N., Druzhbin, D., Myhill, R., Li, Y., Wang, L., Yamamoto, T., Miyajima, N., Kawazoe, T., Nishiyama, N., Higo, Y., Tange, Y., and Katsura, T. (2016). Generation of pressure over 40 GPa using Kawai-type multi-anvil press with tungsten carbide anvils. The Review of Scientific Instruments, 87, 024501-1–024501-6, https://doi.org/10.1063/1.4941716.

Ishii, T., Criniti, G., Ohtani, E., Purevjav, N., Fei, H., Katsura, T., and Mao, H.-K. (2022) Superhydrous aluminous silica phases as major water hosts in high-temperature lower mantle. Proceedings of the National Academy of Sciences of the United States of America, 119, e2211243119, https://doi.org/10.1073/pnas.2211243119.

Johnson, E.A. (2006) Water in nominally anhydrous crustal minerals: Speciation, concentration, and geologic significance. Reviews in Mineralogy and Geochemistry, 62, 117–154, https://doi.org/10.2138/rmg.2006.62.6.

Johnson, E.A. and Rossman, G.R. (2003) The concentration and speciation of hydrogen in feldspars using FTIR and ^{1}H MAS NMR spectroscopy. American Mineralogist, 88, 901–911, https://doi.org/10.2138/am-2003-5-620.

——— (2004) A survey of hydrous species and concentrations in igneous feldspars. American Mineralogist, 89, 586–600, https://doi.org/10.2138/am-2004-0413.

Kaminsky, F. (2012) Mineralogy of the lower mantle: A review of 'super-deep' mineral inclusions in diamond. Earth-Science Reviews, 110, 127–147, https://doi.org/10.1016/j.earscirev.2011.10.005.

Koch-Müller, M. and Rhede, D. (2010) IR absorption coefficients for water in nominally anhydrous high-pressure minerals. American Mineralogist, 95, 770–775, https://doi.org/10.2138/am.2010.3358.

Kohlstedt, D.L. (2006) The role of water in high-temperature rock deformation. Reviews in Mineralogy and Geochemistry, 62, 377–396, https://doi.org/10.2138/rmg.2006.62.16.

Libowitzky, E. (1999) Correlation of O-H stretching frequencies and O-H···O hydrogen bond lengths in minerals. Monatshefte für Chemie, 130, 1047–1059, https://doi.org/10.1007/BF03354882.

Libowitzky, E. and Rossman, G.R. (1996) Principles of quantitative absorbance measurements in anisotropic crystals. Physics and Chemistry of Minerals, 23, 319–327, https://doi.org/10.1007/BF00199497.

——— (1997) An IR absorption calibration for water in minerals. American Mineralogist, 82, 1111–1115, https://doi.org/10.2138/am-1997-11-1208.

Lin, Y., Hu, Q., Meng, Y., Walter, M., and Mao, H.-K. (2020) Evidence for the stability of ultrahydrous stishovite in Earth's lower mantle. Proceedings of the National Academy of Sciences of the United States of America, 117, 184–189, https://doi.org/10.1073/pnas.1914295117.

Lin, Y., Hu, Q., Walter, M.J., Yang, J., Meng, Y., Fang, X., Zhuang, Y., Cohen, R.E., and Mao, H.-K. (2022) Hydrous SiO_2 in subducted oceanic crust and H_2O transport to the core-mantle boundary. Earth and Planetary Science Letters, 594, 117708, https://doi.org/10.1016/j.epsl.2022.117708.

Litasov, K.D., Kagi, H., Shatskiy, A., Ohtani, E., Lakshtanov, D.L., Bass, J.D., and Ito, E. (2007) High hydrogen solubility in Al-rich stishovite and water transport in the lower mantle. Earth and Planetary Science Letters, 262, 620–634, https://doi.org/10.1016/j.epsl.2007.08.015.

Litvin, Y., Spivak, A., Solopova, N., and Dubrovinsky, L. (2014) On origin of lower-mantle diamonds and their primary inclusions. Physics of the Earth and Planetary Interiors, 228, 176–185, https://doi.org/10.1016/j.pepi.2013.12.007.

Liu, L.G. (1986) Phase transformations in serpentine at high pressures and temperatures and implications for subducting lithosphere. Physics of the Earth and Planetary Interiors, 42, 255–262, https://doi.org/10.1016/0031-9201(86)90028-2.

——— (1987) Effects of H_2O on the phase behaviour of the forsterite-enstatite system at high pressures and temperatures and implications for the earth. Physics of the Earth and Planetary Interiors, 49, 142–167, https://doi.org/10.1016/0031-9201(87)90138-5.

Liu, L., Mernagh, T.P., and Hibberson, W.O. (1997) Raman spectra of high-pressure polymorphs of SiO_2 at various temperatures. Physics and Chemistry of Minerals, 24, 396–402, https://doi.org/10.1007/s002690050053.

Liu, L.G., Lin, C.C., Irifune, T., and Mernagh, T.P. (1998) Raman study of phase D at various pressures and temperatures. Geophysical Research Letters, 25, 3453–3456, https://doi.org/10.1029/98GL01415.

Nishi, M., Irifune, T., Tsuchiya, J., Tange, Y., Nishihara, Y., Fujino, K., and Higo, Y. (2014) Stability of hydrous silicate at high pressures and water transport to the deep lower mantle. Nature Geoscience, 7, 224–227, https://doi.org/10.1038/ngeo2074.

Nisr, C., Leinenweber, K., Prakapenka, V., Prescher, C., Tkachev, S., and Shim, S.-H. (2017) Phase transition and equation of state of dense hydrous silica up to 63 GPa. Journal of Geophysical Research: Solid Earth, 122, 6972–6983, https://doi.org/10.1002/2017JB014055.

Ohtani, E. (2005) Water in the mantle. Elements, 1, 25–30, https://doi.org/10.2113/gselements.1.1.25.

——— (2015) Hydrous minerals and the storage of water in the deep mantle. Chemical Geology, 418, 6–15, https://doi.org/10.1016/j.chemgeo.2015.05.005.

Ohtani, E., Litasov, K., Hosoya, T., Kubo, T., and Kondo, T. (2004) Water transport into the deep mantle and formation of a hydrous transition zone. Physics of the Earth and Planetary Interiors, 143-144, 255–269, https://doi.org/10.1016/j.pepi.2003.09.015.

Pamato, M.G., Myhill, R., Boffa Ballaran, T., Frost, D.J., Heidelbach, F., and Miyajima, N. (2015) Lower-mantle water reservoir implied by the extreme stability of a hydrous aluminosilicate. Nature Geoscience, 8, 75–79, https://doi.org/10.1038/ngeo2306.

Panero, W.R., Smyth, J.R., Pigott, J.S., Liu, Z., and Frost, D.J. (2013) Hydrous ringwoodite to 5 k and 35 GPa: Multiple hydrogen bonding sites resolved with FTIR spectroscopy. American Mineralogist, 98, 637–642, https://doi.org/10.2138/am.2013.3978.

Pawley, A.R., McMillan, P.F., and Holloway, J.R. (1993) Hydrogen in stishovite, with implications for mantle water content. Science, 261, 1024–1026, https://doi.org/10.1126/science.261.5124.1024.

Pearson, D.G., Brenker, F.E., Nestola, F., McNeill, J., Nasdala, L., Hutchison, M.T., Matveev, S., Mather, K., Silversmit, G., Schmitz, S., and others. (2014) Hydrous mantle transition zone indicated by ringwoodite included within diamond. Nature, 507, 221–224, https://doi.org/10.1038/nature13080.

Prince, E. (2004) International Tables for Crystallography, Volume C: Mathematical, Physical and Chemical Tables, 1040 p. Wiley.

Purevjav, N., Fei, H., Ishii, T., Criniti, G., Lin, Y., Mao, H-K., and Katsura, T. (2024). Temperature dependence of H_2O solubility in Al-Free stishovite. Geophysical Research Letters, 51, e2023GL104029, https://doi.org/10.1029/2023GL104029.

Saal, A.E., Hauri, E.H., Langmuir, C.H., and Perfit, M.R. (2002) Vapour undersaturation in primitive mid-ocean-ridge basalt and the volatile content of Earth's upper mantle. Nature, 419, 451–455, https://doi.org/10.1038/nature01073.

Sheldrick, G.M. (2018) SHELXL: Programs for crystal structure analysis. University of Göttingen.

Shieh, S.R., Mao, H.-K., Hemley, R.J., and Ming, L.C. (1998) Decomposition of phase D in the lower mantle and the fate of dense hydrous silicates in subducting slabs. Earth and Planetary Science Letters, 159, 13–23, https://doi.org/10.1016/S0012-821X(98)00062-4.

Shieh, S.R., Duffy, T.S., Liu, Z., and Ohtani, E. (2009) High-pressure infrared spectroscopy of the dense hydrous magnesium silicates phase D and phase E. Physics of the Earth and Planetary Interiors, 175, 106–114, https://doi.org/10.1016/j.pepi.2009.02.002.

Shinmei, T., Irifune, T., Tsuchiya, J., and Funakoshi, K. (2008) Phase transition and compression behavior of phase D up to 46 GPa using multi-anvil apparatus with sintered diamond anvils. High Pressure Research, 28, 363–373, https://doi.org/10.1080/08957950802246514.

Smyth, J., Swope, R., and Pawley, A. (1995) H in rutile-type compounds: II. Crystal chemistry of Al substitution in H-bearing stishovite. American Mineralogist, 80, 454–456, https://doi.org/10.2138/am-1995-5-605.

Smyth, J.R., Kawamoto, T., Jacobsen, S.D., Swope, R.J., Hervig, R.L., and Holloway, J.R. (1997) Crystal structure of monoclinic hydrous wadsleyite [β-$(Mg,Fe)_2SiO_4$]. American Mineralogist, 82, 270–275, https://doi.org/10.2138/am-1997-3-404.

Spektor, K., Nylen, J., Stoyanov, E., Navrotsky, A., Hervig, R.L., Leinenweber, K., Holland, G.P., and Häussermann, U. (2011) Ultrahydrous stishovite from high-pressure hydrothermal treatment of SiO2. Proceedings of the National Academy of Sciences of the United States of America, 108, 20918–20922, https://doi.org/10.1073/pnas.1117152108.

Spektor, K., Nylen, J., Mathew, R., Eden, M., Stoyanov, E., Navrotsky, A., Leinenweber, K., and Häussermann, U. (2016) Formation of hydrous stishovite from coesite in high pressure hydrothermal environments. American Mineralogist, 101, 2514–2524, https://doi.org/10.2138/am-2016-5609.

Stachel, T., Brey, G.P., and Harris, J.W. (2005) Inclusions in sublithospheric diamonds: Glimpses of deep Earth. Elements, 1, 73–78, https://doi.org/10.2113/gselements.1.2.73.

Takaichi, G., Nishihara, Y., Matsukage, K.N., Nishi, M., Higo, Y., Tange, Y., Tsujino, N., and Kakizawa, S. (2024). Limited stability of hydrous SiO_2 stishovite in the deep mantle. Earth and Planetary Science Letters, 640, 118790, https://doi.org/10.1016/j.epsl.2024.118790.

Thomas, S-M., Wilson, K., Koch-Müller M., Hauri, E.H., McCammon, C., Jacobsen, S.D.; Lazarz, J., Rhede, D., Ren, M., Blair, N., and Lenz, S. (2015). Quantification of water in majoritic garnet. American Mineralogist, 100, 1084–1092, https://doi.org/10.2138/am-2015-5136.

Tsuchiya, J. and Umemoto, K. (2019) First-principles determination of the dissociation phase boundary of phase H $MgSiO_4H_2$. Geophysical Research Letters, 46, 7333–7336, https://doi.org/10.1029/2019GL083472.

Tsutsumi, Y., Sakamoto, N., Hirose, K., Tagawa, S., Umemoto, K., Ohishi, Y., and Yurimoto, H. (2024) Retention of water in subducted slabs under core-mantle boundary conditions. Nature Geoscience, 17, 697–704, https://doi.org/10.1038/s41561-024-01464-8.

Williams, Q. and Hemley, R.J. (2001) Hydrogen in the deep Earth. Annual Review of Earth and Planetary Sciences, 29, 365–418, https://doi.org/10.1146/annurev.earth.29.1.365.

Xu, C. and Inoue, T. (2019) Melting of Al-rich phase D up to the uppermost lower mantle and transportation of H_2O to the deep Earth. Geochemistry, Geophysics, Geosystems, 20, 4382–4389, https://doi.org/10.1029/2019GC 008476.

Yang, H., Prewitt, C.T., and Frost, D.J. (1997) Crystal structure of the dense hydrous magnesium silicate, phase D. American Mineralogist, 82, 651–654, https://doi.org/10.2138/am-1997-5-627.

Zhang, L., Smyth, J.R., Kawazoe, T., Jacobsen, S.D., Niu, J.J., He, X.J., and Qin, S. (2019) Stability, composition, and crystal structure of Fe-bearing phase E in the transition zone. American Mineralogist, 104, 1620–1624, https://doi.org/10.2138/am-2019-6750.

Zhu, L., Chen, R.-X., Zheng, Y.-F., Wang, J., and Gong, B. (2023) Calibration of infrared absorption coefficients for structural hydroxyl in garnet by a combined study of isotope ratio spectrometry and vibrational spectroscopy. Geostandards and Geoanalytical Research, 47, 105–124, https://doi.org/10.1111/ggr.12461.

Manuscript received October 29, 2024
Manuscript accepted April 2, 2025
Accepted manuscript online April 8, 2025
Manuscript Handled by Antonio M. dos Santos

Endnotes:

[1]Deposit item AM-25-119665. Online Materials are free to all readers. Go online, via the table of contents or article view, and find the tab or link for supplemental materials. The CIF has been peer-reviewed by our Technical Editors.